Research Square

Preprints are preliminary reports that have not undergone peer review.
They should not be considered conclusive, used to inform clinical practice,
or referenced by the media as validated information.

A Phase-Field Assessment of Hydrogen-Assisted Fatigue Crack Growth in X52 Pipeline Steel: Three-Stage Crack Evolution and Hydrogen Concentration Trends

Xiaolin Ma
Xinjiang University
Ziliang Shi
Dongfang Electric (Fujian) Innovation Institute Co., Ltd
Geli Mao
Xinjiang University
Yaxin Zhang
181679557260163.com

Xinjiang University
Tao Yang
Xinjiang University

Research Article

Keywords: Hydrogen pipeline, Phase-field method, Fatigue crack propagation, Hydrogen concentration, Critical energy release rate, X52 pipeline steel

Posted Date: September 22nd, 2026

DOI: https://doi.org/10.21203/rs.3.rs-10892870/v1

License: This work is licensed under a Creative Commons Attribution 4.0 International License.
Read Full License

Additional Declarations: No competing interests reported.

A Phase-Field Assessment of Hydrogen-Assisted Fatigue Crack Growth in X52 Pipeline Steel: Three-Stage Crack Evolution and Hydrogen Concentration Trends

Xiaolin Ma[1,3], Ziliang Shi[2], Geli Mao [1,3], Yaxin Zhang [1,3,*], Tao Yang [1,3]

1. School of Chemical Engineering, Xinjiang University, Xinjiang 830017, China;

2. Dongfang Electric (Fujian) Innovation Institute Co., Ltd, Fuzhou, Fujian, 350001, China;

3. State Key Laboratory of Chemistry and Utilization of Carbon-Based Energy Resources, Xinjiang University, Xinjiang 830017, China

Corresponding Author: ZHANG Yaxin

Email Address: 18167955726@163.com

Affiliation: School of Chemical Engineering and Technology, Xinjiang University

ABSTRACT

Hydrogen embrittlement significantly accelerates fatigue crack growth in pipeline steels, threatening the safe operation of hydrogen transmission pipelines. A coupled phase-field model integrating hydrogen diffusion, fatigue degradation, and brittle fracture is used to investigate hydrogen-assisted fatigue crack propagation in X52 pipeline steel under internal pressure fluctuations. The process comprises three stages—energy accumulation, accelerated growth, and rapid fracture—accounting for approximately 20%, 72%–74%, and 3%–6% of the simulated fatigue life under the adopted stage definitions. The relative hydrogen concentration in the crack-tip region peaks at crack initiation (point N2) and then decreases. In the present model, the maximum hydrogen concentration occurs approximately 0.1–0.2 mm ahead of the crack tip, and this distance increases with crack growth and hydrogen pressure. The relative critical energy release rate decreases with crack extension; within the linear-elastic pressure range considered, degradation peaks in Stage II. Within the linear-elastic pressure range, the model indicates that higher hydrogen pressure promotes earlier degradation, whereas fatigue effects dominate during the prolonged propagation stage. These model-based findings illustrate trends under the stated assumptions and are not validated quantitative criteria for predicting the fatigue life of hydrogen pipelines.

Keywords: Hydrogen pipeline; Phase-field method; Fatigue crack propagation; Hydrogen concentration; Critical energy release rate; X52 pipeline steel

1. Introduction

Hydrogen energy is widely regarded as a key driver of global decarbonization strategies because of its abundant reserves, cleanliness, and versatile applications [1]. However, the widespread adoption of hydrogen energy faces a critical challenge: hydrogen embrittlement [2]. The ingress of hydrogen into metallic materials significantly alters their fracture resistance, ductility, and fatigue crack growth rate [3], [4], [5], with changes reaching several orders of magnitude. This phenomenon is of particular concern for hydrogen transmission pipelines, because pipeline materials experience alternating mechanical loads in service, creating conditions for synergistic hydrogen embrittlement and fatigue damage [6], [7].

Extensive experimental studies have confirmed that hydrogen significantly accelerates the fatigue crack growth in pipeline steels [8], [9].Research has shown that the fatigue crack growth rate of X52 pipeline steel in high-pressure hydrogen environments is substantially higher than that in air, typically by one to two orders of magnitude. The main influencing factors include hydrogen pressure, stress ratio (R), loading frequency, and temperature[10], [11], [12].However, experimental methods are inherently limited in resolving the complex multi-physics interactions at the crack tip, especially the coupled evolution of the stress field, hydrogen concentration, and material degradation. Traditional linear elastic fracture mechanics and cohesive zone models can provide valuable insight into hydrogen-assisted fracture, but they struggle to capture the complex behaviour in hydrogen environments[13]. These methods typically rely on predefined crack paths and cannot naturally simulate crack initiation, branching, or the dynamic coupling between hydrogen diffusion and fracture [14], [15].In recent years, the phase-field method has emerged as a powerful computational tool for fracture modelling, offering significant advantages over discrete fracture approaches [16].Unlike approaches that explicitly track crack surfaces, the phase-field method

represents cracks as a continuous scalar field, enabling the natural simulation of complex fracture processes, including crack nucleation, propagation, coalescence, and branching[17]. Its variational framework is rooted in Griffith's fracture theory [18], providing a thermodynamically consistent description of crack evolution.

Cui et al.[19] developed a comprehensive phase-field model for hydrogen-assisted fatigue that integrates fracture and fatigue descriptions with stress-assisted hydrogen diffusion and toughness degradation. Their predictions show good agreement with experimental data across various load ratios, hydrogen pressures, and loading frequencies, without requiring calibration specifically for hydrogen-assisted fatigue data. Golahmar et al. [20] proposed the first phase-field theoretical framework for hydrogen-assisted fatigue, systematically elucidating the competition between loading frequency and hydrogen diffusion on crack growth rates. Their formulation successfully reproduced Paris-law behaviour and virtual S-N curves. Liu et al. [21] further established a unified variational phase-field framework that couples mechanical deformation, hydrogen diffusion, and cyclic fatigue damage, systematically revealing the synergistic effects of hydrogen concentration and loading frequency on fatigue crack propagation life. Kristensen et al. [22] provided a comprehensive review of phase-field applications in modelling hydrogen-assisted failures, highlighting the capability of the method to capture complex cracking phenomena such as nucleation from multiple sites and coalescence of numerous defects. Although these models have successfully captured key features of hydrogen-assisted fatigue in general settings, their application to pipeline-specific geometries and loading conditions remains limited.

Despite these advances, several aspects relevant to engineering applications involving pipeline steels under internal pressure fluctuations remain insufficiently investigated. First, the interaction between the crack-tip stress field and hydrogen diffusion under cyclic loading has not been systematically characterised, particularly the migration of the maximum stress point relative to the advancing crack tip. Second, although existing models have predicted fatigue crack growth rates, the three-stage evolution of the propagation process—from energy accumulation to accelerated growth and rapid fracture—and its dependence on hydrogen pressure and stress ratio remain unclear. Third, the degradation of the critical energy release rate at different propagation stages and the relative contributions of hydrogen embrittlement and pure fatigue damage to material degradation have yet to be quantified.

This study aims to fill these gaps by using a coupled phase-field-diffusion-fatigue framework to investigate hydrogen-assisted fatigue crack propagation in X52 pipeline steel under internal pressure loading. The specific objectives are (1) to characterise the three-stage evolution of fatigue crack propagation and quantify the duration of each stage under various hydrogen pressures and stress ratios; (2) to characterise the migration behaviour of the maximum stress point relative to the crack tip and its dependence on hydrogen pressure and crack extension in the model; (3) to quantify the degradation behaviour of the critical energy release rate under coupled hydrogen-fatigue effects; and (4) to illustrate the possible contributions of hydrogen and fatigue to material degradation at different stages of crack propagation. The findings provide model-based trends within the linear-elastic pressure range and are not intended as validated quantitative criteria for pipeline integrity assessment.

2. Phase-Field Model Formulation

2.1 **Hydrogen diffusion theory and hydrogen degradation function**

The diffusion of hydrogen into metallic materials in a hydrogen-containing environment follows the law of mass conservation, which relates the rate of change of hydrogen concentration C to the hydrogen flux through the external surface. For a body of volume Ω and surface area S, the integral form of the hydrogen diffusion governing equation is given by[23]:

$$\int_{\Omega} \frac{dC}{dt} dV + \int_{\partial\Omega} \mathbf{J} \cdot \mathbf{n} dS = 0 \tag{1}$$

Applying the divergence theorem, the strong form of Eq. (1) is obtained as

$$\frac{dC}{dt} + \nabla \cdot \mathbf{J} = 0 \tag{2}$$

The mass flux J obeys the linear Onsager relation:

$$\mathbf{J} = -\frac{DC}{R_g T} \nabla \mu \tag{3}$$

$$\mu = \mu^0 + R_g T \ln \frac{\theta_L}{1-\theta_L} - \bar{V}_H \sigma_H \tag{4}$$

where D is the hydrogen diffusion coefficient, C is the hydrogen concentration, Rg is the gas constant, T is the absolute temperature, ∇μ is the driving force of the chemical potential, μ^0 is the chemical potential at the standard state, θ_L is the lattice site occupancy, θ_L = c/N, and σ_H is the hydrostatic stress.

When the lattice occupancy is very low and the concentration of interstitial sites is constant (∇N = 0), the mass flux **J** can be expressed as:

$$\mathbf{J} = -D\nabla C + \frac{DC}{R_g T} \bar{V}_H \nabla \sigma_H \tag{5}$$

Therefore, the critical energy release rate in a hydrogen environment can be related to the hydrogen coverage θ [24], [25]:

$$f_C(C) = 1 - \chi^{\theta} \tag{6}$$

where χ is the damage coefficient quantifying the reduction in fracture energy caused by hydrogen.

The hydrogen coverage θ is related to the hydrogen concentration by the following expression:

$$\theta = \frac{C}{C + \exp\left(\frac{-\Delta g_b^0}{R_g T}\right)} \tag{7}$$

where Δg_b^0 is the Gibbs free energy for hydrogen segregation, taken as 30 kJ/mol.

2.2 **Fatigue degradation theory**

When a material undergoes fatigue, its mechanical properties deteriorate; that is, fatigue damage accumulates. Fatigue damage is represented by a degradation function of the form:

$$f_{\bar{\alpha}}(\bar{\alpha}) = \begin{cases} 1 & if \quad \bar{\alpha} \le \alpha_T \\ \left(\frac{2\alpha_T}{\bar{\alpha} + \alpha_T}\right)^2 & if \quad \bar{\alpha} > \alpha_T \end{cases} \qquad (Asymptotic) \tag{8}$$

Where $\bar{\alpha}$ is the accumulated history variable, $\bar{\alpha} = g(\phi)\psi_0$; α_T is the fatigue threshold parameter, $\alpha_T = \frac{G_c}{12l}$. G_c is the critical energy release rate for crack propagation.

$$\bar{\alpha}(t) = \int_0^t H(\alpha\dot{\alpha})|\dot{\alpha}|\,dt \tag{9}$$

where H denotes the Heaviside function, which ensures that crack growth occurs only during cyclic loading and that no crack healing is permitted.

2.3 **Phase-field description of crack evolution**

The phase-field method introduces an auxiliary scalar field, the phase field φ, to represent the crack topology [26]. In a one-dimensional setting, the topology of a sharp crack can be described by the auxiliary field variable $\phi(x)$:

$$\phi(x) = \exp\left(\frac{-|x-a|}{l_0}\right) \tag{10}$$

where a denotes the crack position and l_0 is the length scale that controls the degree of crack diffusion; $\phi = 0$ and $\phi = 1$ represent the intact and fully fractured states of the material, respectively.

Extending Eq. (11) to two and three dimensions, the crack surface density function is introduced as:

$$\gamma(\phi) = \frac{1}{2}\left[l_0 \nabla^2 \phi + \frac{1}{l_0}\phi^2\right] \tag{11}$$

The regularised surface energy is then given by:

$$\psi^s = \int_\Omega \frac{G_c(\theta)}{2}\left[l_0 \nabla^2 \phi + \frac{1}{l_0}\phi^2\right] d\Omega \tag{12}$$

A stress degradation function $g(\phi)=(1-\phi)^2+k$ is introduced, where k is a small positive parameter used to avoid numerical singularities. Thus, the strain energy density, accounting for the influence of the phase field, becomes:

$$\psi^b=\int_\Omega\left[(1-\phi)^2+k\right]\psi_e(\varepsilon)d\Omega \tag{13}$$

The total potential energy functional is expressed as:

$$\psi(\phi,u)=\psi^s+\psi^b \tag{14}$$

From this, the governing equations for the displacement field and the phase field in quasi-static fracture can be derived [27]:

$$\begin{cases} g(\phi)\nabla\cdot\boldsymbol{\sigma}+\mathbf{b}=0 \\ G_d\left(\dfrac{\phi}{l_0}-l_0\nabla^2\phi\right)-2(1-\phi)\psi(\varepsilon)=0 \\ g(\phi)\boldsymbol{\sigma}\cdot\mathbf{n}=f \\ \nabla\phi\cdot\mathbf{n}=0 \end{cases} \tag{15}$$

$$G_d=f_C(C)f_{\bar{\alpha}}(\bar{\alpha})G_{(0)} \tag{16}$$

where σ is the stress tensor and **n** is the outward unit normal vector to the surface.

3. Model Setup and Validation

3.1 Model Geometry and Boundary Conditions

A three-dimensional pipe model is used to simulate hydrogen-assisted fatigue crack propagation in X52 pipeline steel under internal pressure fluctuations. The pipe has an inner radius of 217.5 mm, a wall thickness of 11 mm, and a length of 500 mm, as shown in Figure 1(a). A semi-elliptical axial crack is introduced on the inner pipe surface with an initial depth $a_0=1.1$ mm and half-length $c_0=1.1$ mm, corresponding to an aspect ratio $a/c=1.0$ and a relative depth $a/t=0.1$, as shown in Figure 1(b), where t; the model remains three-dimensional, and field quantities are presented along a plane section through the wall thickness for visualisation, as shown in Figure 1(d).

The material is X52 pipeline steel with a Young's modulus of $E=200$ GPa, Poisson's ratio $\nu=0.3$, and an initial critical energy release rate of $G_c=2700$ N/m [28]. Four hydrogen pressure levels are considered: 5.5, 6.89, 21, and 34 MPa. A constant maximum pressure is maintained throughout the cyclic loading, with a baseline stress ratio $R=0.8$ and a loading frequency $f=1$ Hz. Additional simulations are conducted at $R=0.5$,0.7, and 0.9 to investigate the effect of stress ratio. The material and model parameters used in the simulations are summarised in Table 1.

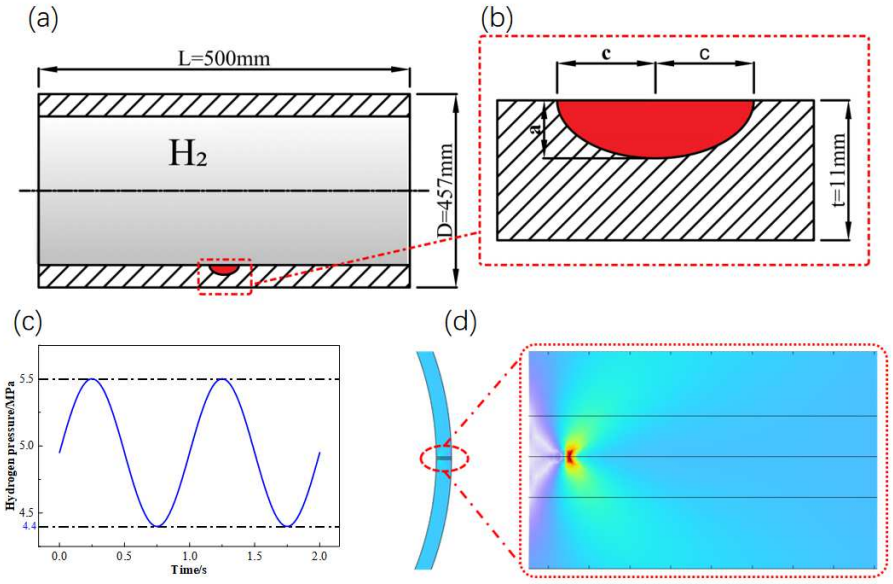


Figure 1 Schematic diagrams: (a) pipeline; (b) crack model; (c) fluctuations in hydrogen pressure within pipelines; (d) plane-section visualisation of cracks along the wall-thickness direction

Table 1 Material and model parameters used in the simulations

Parameter	Value
Young's modulus E/GPa	200
Poisson's ratio v	0.3
Minimum yield strength sys/MPa	360
Temperature T/K	300
Hydrogen diffusivity D/(mm^2/s)	0.0127
Initial critical energy release rate Gc/(N/m)	2700
Phase-field length l_0/mm	0.1
Regularisation parameter k	1E-7
Hydrogen damage coefficient χ	0.89
Gibbs free energy g_b^0 /(kJ/mol)	30
Hydrogen partial molar volume $\overline{V}_H$ /(mm^3/mol)	2.0×10^3

3.2 Boundary and Loading Conditions

3.2.1 Hydrogen Concentration Boundary Conditions

The pipe is assumed to be pre-charged with hydrogen and continuously exposed to a hydrogen-containing environment during the full fatigue test. The surface hydrogen concentration at the inner wall and crack faces is determined by Sievert's law:

$$C_{surf} = \mathrm{S}\sqrt{p_{H_2}} \tag{17}$$

where $S = 0.077 wt.ppm \cdot MPa^{-0.5}$ is the hydrogen solubility in X52 steel [19] and p_{H_2} is the hydrogen partial pressure (in MPa). The four hydrogen pressures yield surface concentrations of approximately 0.18, 0.20, 0.35, and 0.45 wt ppm for 5.5, 6.89, 21, and 34 MPa, respectively. A Dirichlet boundary condition $C = C_{\text{surf}}$ is applied on the inner pipe surface and crack faces, and a zero-flux condition $J \cdot n = 0$ is imposed on the outer pipe surface.

3.2.2 Cyclic Loading Condition

A sinusoidal pressure waveform is adopted to simulate the cyclic internal pressure experienced by in-service pipelines:

$$\mathrm{p}(\mathrm{t}) = p_{max}\left[R + (1-R)sin^2(\frac{\pi t}{T})\right] \tag{18}$$

where $p_{max}\ and\ p_{min}$ are the maximum, minimum pressure respectfully, $R = \frac{p_{min}}{p_{max}}$ is the stress ratio, and $\mathrm{T} = \frac{1}{f}$ is the loading period. The stress ratio is defined with the maximum pressure held constant to better represent actual pipeline operating conditions [29]. A baseline stress ratio of R=0.8 is adopted, with additional simulations at R=0.5, 0.7, and 0.9.

The loading frequency is set to $f = 1$ Hz, which is sufficiently low to allow hydrogen diffusion to approach equilibrium during each loading cycle [20], [25]. Fatigue evolution is tracked as a function of the cumulative cycle count N. In the reference cyclic loading representation, 20 uniform load increments per cycle are used, and a convergence study confirmed that refining the temporal resolution (e.g., 40 increments per cycle) alters the predicted fatigue life by less than 2%.

To keep the high-cycle cases tractable, the fatigue history variable is integrated in the cycle-count coordinate, so fatigue life is reported in terms of N rather than physical loading time.

3.3 Mesh Sensitivity Analysis and Validation

3.3.1 Mesh Sensitivity Analysis

The mesh sensitivity is evaluated by refining the crack region with minimum element sizes $h = \frac{l_0}{5.4}$, $\frac{l_0}{5.6}$, $\frac{l_0}{5.8}$ and $\frac{l_0}{6.0}$ corresponding to total element counts of 478467, 525218, 583974, and 638941, respectively. As shown in Figure 2, when $h \le \frac{l_0}{5.8}$ (element count = 583,974), the variation in relative hydrogen concentration $\frac{C}{C_0}$ is less than 1%. The predicted fatigue crack propagation life also converges at this refinement level, with further mesh refinement altering the life prediction by less than 3%. Considering both accuracy and computational

efficiency, a mesh with $h = \frac{l_0}{5.8}$ is adopted for all subsequent simulations.

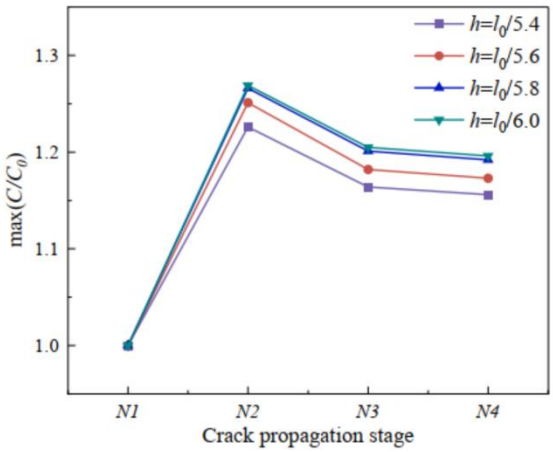


Figure 2 Mesh sensitivity analysis: relative hydrogen concentration versus normalized crack length

3.3.2 Assessment of Numerical Feasibility

To assess the numerical feasibility of the present coupled phase-field implementation, the predicted fatigue crack growth behaviour is benchmarked against the reference data reported in under the same model configuration [26]. Specifically, the simulated crack length versus number of cycles is compared with the reference crack-growth data. The comparison shown in Figure 3 demonstrates that the present implementation reproduces the reference evolution within 5%. This benchmark confirms the numerical feasibility of the baseline fatigue implementation; it does not validate the hydrogen-assisted fatigue predictions for X52 pipeline steel.

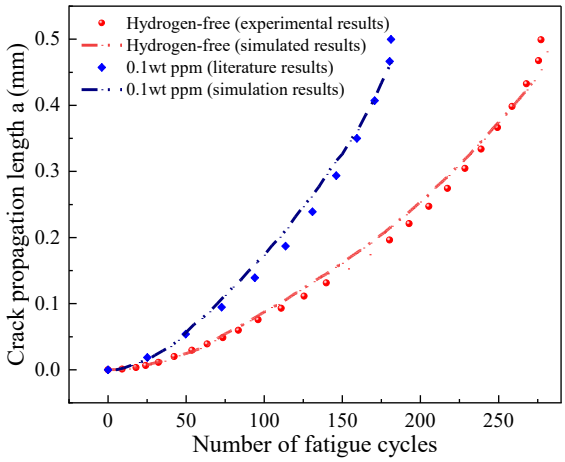


Figure 3 Verification of simulation accuracy: comparison between predicted and reference crack growth

4. Results and Discussion

4.1 Three-Stage Fatigue Crack Propagation Process

Figure 4 presents the fatigue crack propagation depth as a function of the number of cycles under hydrogen pressures of 5.5, 6.89, 21, and 34 MPa. On the basis of the crack growth rate, the fatigue crack propagation process can be divided into three distinct stages:

Stage I (energy accumulation, N1 → N2, where N1 denotes the initial loading state at N = 0): The crack does not propagate, but the material strength gradually degrades under combined hydrogen and fatigue effects. The end of Stage I (point N2) is defined as the cycle count at which the crack first extends beyond 0.01 mm.

Stage II (accelerated propagation, N2 → N4): The crack initiates at point N2and propagates with an accelerating growth rate. Point N4 is defined as the transition point where $\mathrm{d}^2a/\mathrm{d}N^2$ changes sign (i.e., the inflection point of the a–N curve), marking the onset of rapid fracture.

Stage III (rapid fracture, N4 → N5): The crack propagates rapidly until final fracture (point N5), defined as the cycle count at which the crack penetrates the entire wall thickness.

Figure 5 shows the phase-field contours at points N2, N3, and N4, illustrating the evolution of the crack phase field during propagation.

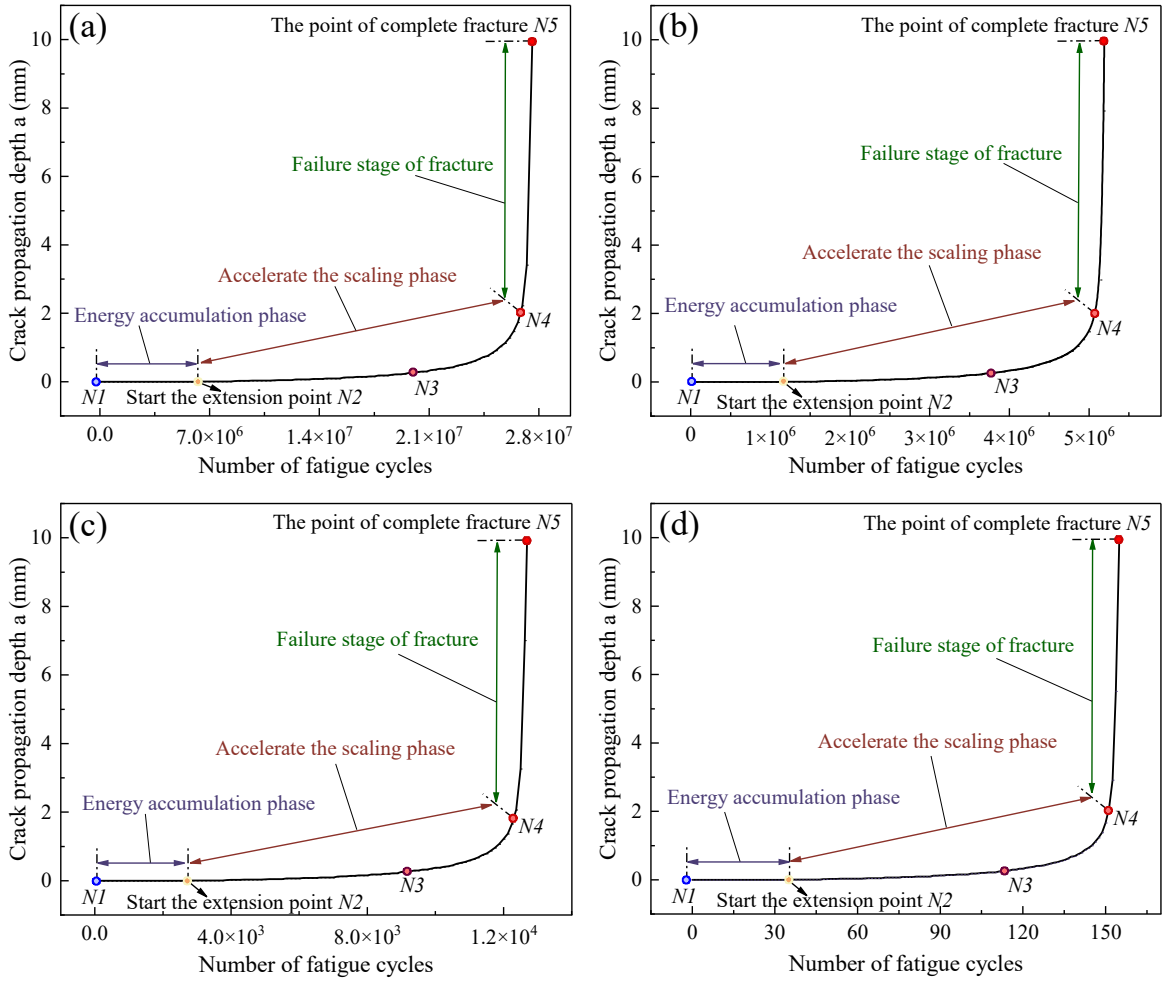


Figure 4 Fatigue crack propagation process under different hydrogen pressures: (a) 5.5 MPa; (b) 6.89 MPa; (c) 21 MPa; (d) 34 MPa



Figure 5 Phase-field contours at different stages: (a)N2(b)N3(c)N4

Tables 2 and 3 summarise the fatigue cycle counts at each characteristic point and the percentage of each stage. Across the hydrogen pressures and stress ratios considered, the three stages account for approximately 20% (Stage I), 72%–74% (Stage II), and 3%–6% (Stage III) of the simulated fatigue life. The small variations, especially the Stage III range of 2.6%–5.8%, indicate that the proportions depend on the chosen stage thresholds and should be regarded as a model-based observation under the present definitions rather than an intrinsic material property or design-life fraction.

Under the present 0.01 mm definition of crack initiation, the model suggests that the first approximately 20% of the simulated life contains no crack extension beyond this threshold. This criterion is definition-dependent and should not be interpreted as a directly measurable safe inspection interval without experimental validation.

Table 2 Three-stage fatigue cycle distribution at different hydrogen pressures (R = 0.8)

H_2 pressure (MPa)	*N*2	*N*3	*N*4	*N*5	Stage I(%)	Stage II(%)	Stage III(%)
5.5	6.20×10^6	20.56×10^6	26.03×10^6	27.58×10^6	22.48	71.90	5.62
6.89	1.21×10^6	3.79×10^6	5.07×10^6	5.27×10^6	22.96	73.24	3.80
21	2.85×10^3	9.25×10^3	12.28×10^3	12.79×10^3	22.28	73.73	3.99
34	35	114	151	156	21.79	74.36	3.85

Table 3 Three-stage fatigue cycle distribution at different stress ratios (p = 5.5 MPa)

R	*N*2	*N*3	*N*4	*N*5	Stage I(%)	Stage II(%)	Stage III(%)
0.5	2.36×10^6	7.91×10^6	9.82×10^6	10.08×10^6	23.41	73.31	2.58
0.7	4.21×10^6	13.94×10^6	17.58×10^6	18.66×10^6	22.56	71.65	5.79
0.8	6.20×10^6	20.56×10^6	26.03×10^6	27.58×10^6	22.48	71.90	5.62
0.9	13.26×10^6	43.83×10^6	55.34×10^6	58.51×10^6	22.66	71.92	5.42

The three-stage evolution observed here is qualitatively consistent with the fatigue crack growth behaviour predicted by Golahmar et al. [20] and Liu et al. [21], both of which reported accelerating crack growth rates under cyclic loading. However, neither study explicitly quantified the proportional duration of each stage or investigated

its dependence on hydrogen pressure and stress ratio. The present results thus provide a systematic model-based characterisation of the three-stage process under the stated assumptions, demonstrating internal consistency across the studied conditions rather than experimental validation.

4.2 Hydrogen Concentration Field Evolution

Under stress, hydrogen diffuses toward and accumulates in regions of stress concentration, leading to material degradation. Figure 6 shows the distribution of relative hydrogen concentration C/C_0 along the crack propagation direction at stages N2, N3, and N4 under 5.5 MPa hydrogen pressure. At point N2 (crack initiation, 6.20×10^6 cycles), C/C_0 reaches a maximum of 1.266. At point N3 (20.56×10^6 cycles, crack extension 0.3 mm), C/C_0 decreases to 1.201. At point N4 (26.03×10^6 cycles, crack extension 2 mm), C/C_0 further decreases to 1.192. These results indicate that, in the present model, hydrogen concentration peaks at the moment of crack initiation and then gradually decreases as the crack propagates. The underlying mechanism is that the stress concentration that drives hydrogen accumulation moves ahead of the advancing crack tip, leaving behind a region of reduced hydrostatic stress and thus lower hydrogen concentration.

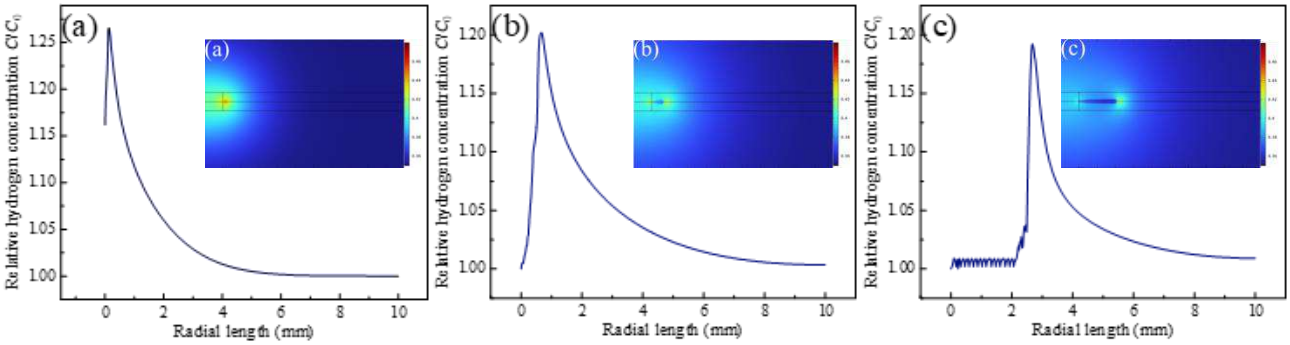


Figure 6 Hydrogen concentration distribution along the crack propagation direction at stages (a) N2, (b) N3, and (c) N4 under 5.5 MPa hydrogen pressure

Figure 7 shows the evolution of the maximum relative hydrogen concentration at each stage under different hydrogen pressures. As hydrogen pressure increases, the peak C/C_0 increases significantly. For all pressures, C/C_0 follows the same trend: it increases to a maximum at N2 and then decreases. Higher hydrogen pressures produce higher relative concentrations at all stages.

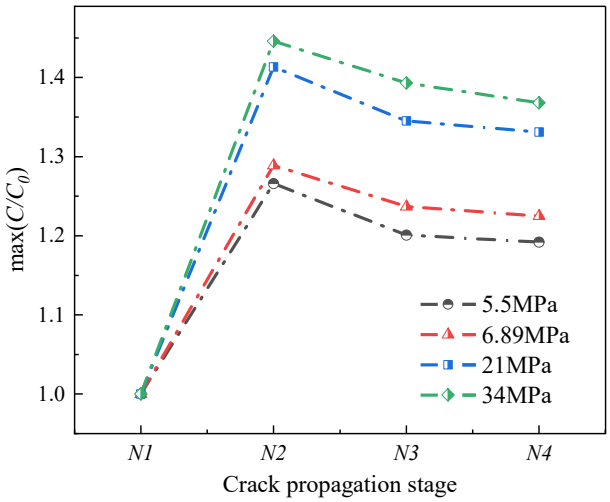


Figure 7 Evolution of relative hydrogen concentration at each stage of crack propagation under different hydrogen pressures

4.3 Stress Field Characteristics and Migration Phenomenon

A notable observation is that the maximum hydrogen concentration is not located exactly at the crack tip, but slightly ahead of it. Figure 8 schematically illustrates the distance d between the crack tip and the location of maximum hydrogen concentration. This phenomenon arises because hydrogen atoms migrate along the stress gradient toward the stress concentration region, which lies ahead of the crack tip due to stress redistribution.

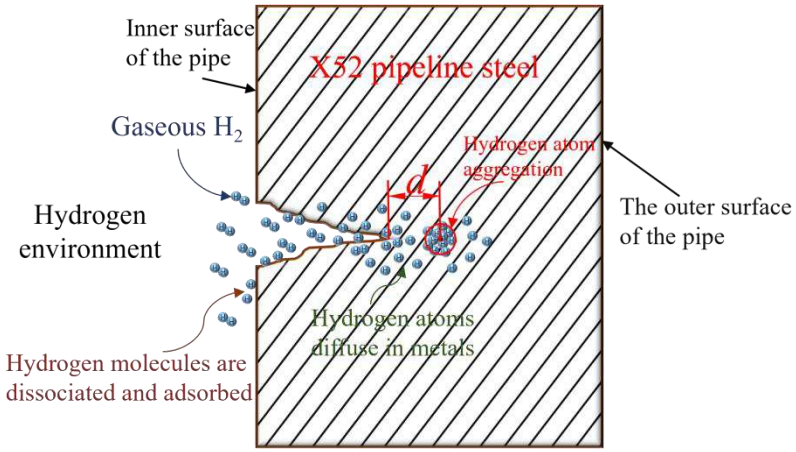


Figure 8 Schematic diagram of the maximum hydrogen concentration and crack-tip location

Figure 9 shows stress contours at stages N2, N3, and N4. As the crack propagates, the stress intensity in the crack-tip region increases, leading to an accelerating crack growth rate.

Figure 10 presents the relationship between stress and phase-field value along the crack propagation direction. The crack tip is defined where $\varphi = 0.95$; the sensitivity of this choice is examined below using alternative thresholds. At N2, the maximum stress is located 0.101 mm ahead of the crack tip. At N3 and N4, this distance d increases to 0.190 mm and 0.199 mm, respectively.

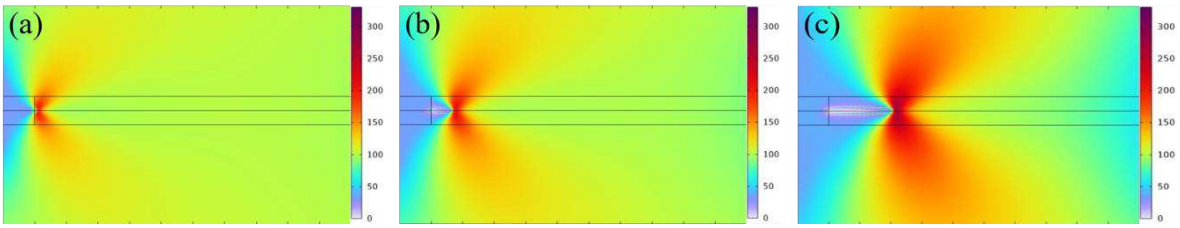


Figure 9 Stress contours at different crack stages under 5.5 MPa hydrogen pressure (a) N2, (b) N3, and (c) N4

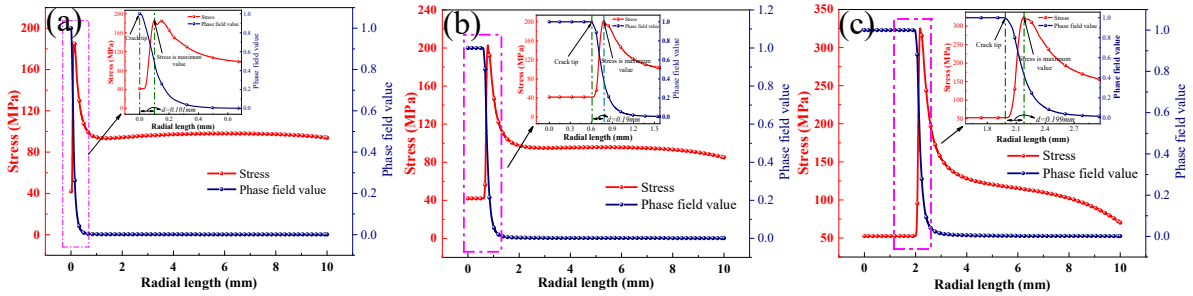
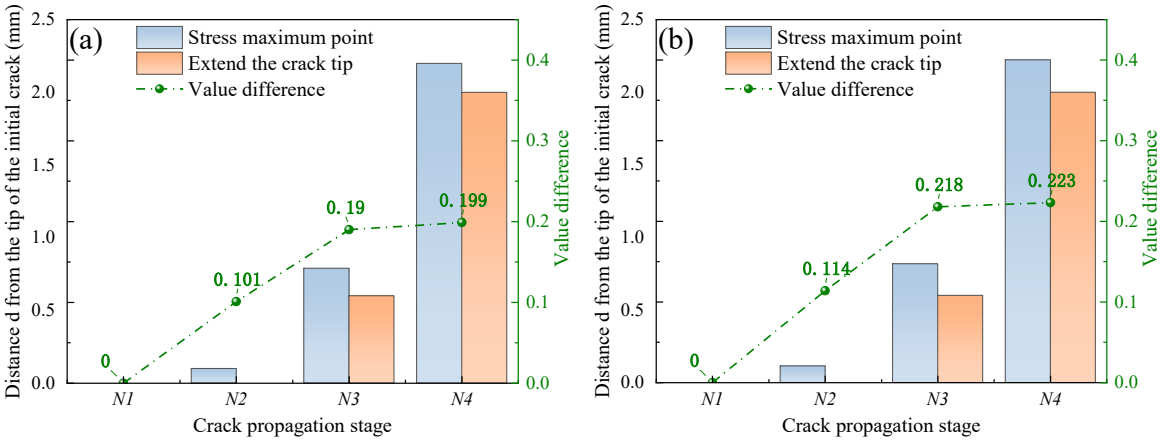


Figure 10 Distributions of stress and phase field values at different stages under 5.5 MPa hydrogen pressure (a) N2, (b) N3, and (c) N4

Within the phase-field regularization scale considered here, the migration distance d increases with crack growth rate and hydrogen pressure. Since the present model assumes linear elastic behaviour without plasticity, this phenomenon cannot be attributed to plastic blunting. Instead, it is interpreted as a consequence of **stress redistribution** ahead of the propagating crack: as the crack advances, the peak hydrostatic stress shifts forward, and the migrating stress concentration draws hydrogen toward the new peak location. In the present fields, the increase in migration distance with hydrogen pressure reflects the enhanced stress-assisted diffusion at higher hydrogen concentrations.

Figure 11 shows the distances from the initial crack tip to the current crack tip and to the maximum stress point under different hydrogen pressures. Both distances increase with hydrogen pressure. For the same hydrogen pressure, the migration distance d increases with crack propagation, but the rate of increase diminishes, suggesting that a steady-state distribution is approached at longer crack lengths.



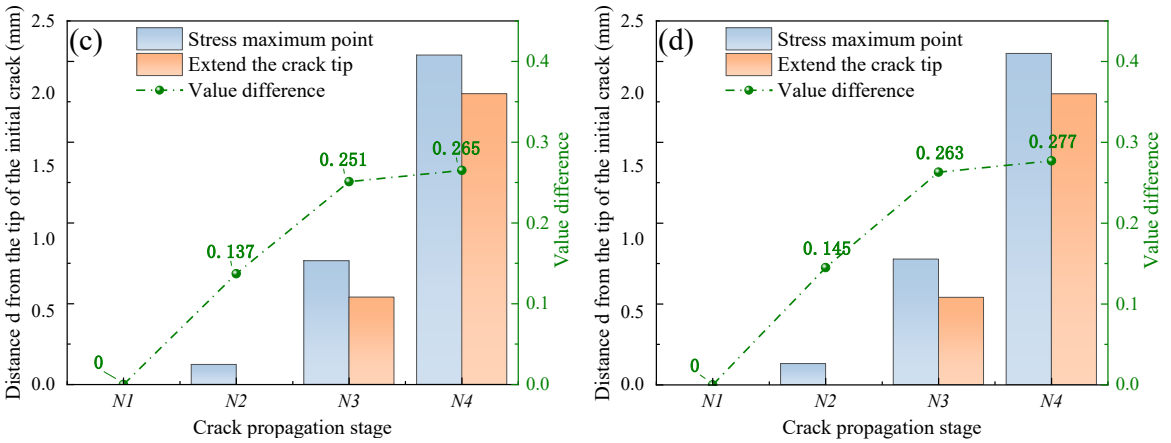


Figure 11 Distance between the crack tip and the maximum stress point from the initial crack under hydrogen pressures of (a) 5.5 MPa, (b) 6.89 MPa, (c) 21 MPa, and (d) 34 MPa

The choice of $\varphi = 0.95$ to define the crack tip is based on the convention in phase-field fracture modelling. To assess the sensitivity of the reported migration distances to this threshold, alternative definitions at $\varphi = 0.90$ and $\varphi = 0.98$ were examined. The resulting migration distances varied by less than 8%, confirming that the observed trends are robust with respect to the exact choice of threshold.

The stress-driven migration of the hydrogen concentration peak has been predicted in the boundary layer model of Golahmar et al. [20], who showed that the hydrogen concentration ahead of a stationary crack tip depends strongly on the loading frequency and diffusivity. The present results extend these findings to propagating cracks in a pipe geometry, showing that the migration distance increases with crack extension and hydrogen pressure in the present phase-field fields. This comparison supports the stress-assisted diffusion mechanism captured by the model but does not establish the migration distances as measured physical lengths; their dependence on the phase-field length scale has not been tested.

4.4 Critical Energy Release Rate Degradation

Hydrogen degrades the critical energy release rate of metallic materials, and fatigue cycling further exacerbates this degradation. In this section, the evolution of the relative critical energy release rate G_d/G_0 during fatigue crack propagation is analysed to quantify the combined effect of hydrogen and fatigue on material degradation.

Figure 12 shows the variation of the relative critical energy release rate G_d/G_0 along the crack propagation direction at stages N2, N3, and N4 under 5.5 MPa hydrogen pressure. At crack initiation (N2), G_d/G_0 approaches zero at the crack tip. This is a direct mathematical consequence of the phase-field formulation: as $\varphi \to 1$, the material is fully cracked and the local fracture resistance vanishes. The physically meaningful quantity is the **maximum** G_d/G_0 along the ligament ahead of the crack tip, which is approximately 0.81 at N2. This indicates that, at the onset of crack propagation, hydrogen has already reduced the critical energy release rate by about **19%** compared with a hydrogen-free environment, demonstrating that hydrogen diffusion to the crack-tip region is largely completed during Stage I. As the crack propagates from N2 to N3 and then to N4, the maximum G_d/G_0 along the ligament decreases progressively to approximately 0.55 and 0.21, respectively. This

continuous reduction reflects the combined effect of ongoing fatigue damage accumulation and sustained hydrogen-assisted degradation ahead of the advancing crack tip. Notably, the reduction is most pronounced in Stage II (from N2 to N4), which accounts for approximately 75% of the total fatigue life, indicating that the accelerated propagation stage is accompanied by substantial material degradation across the ligament.

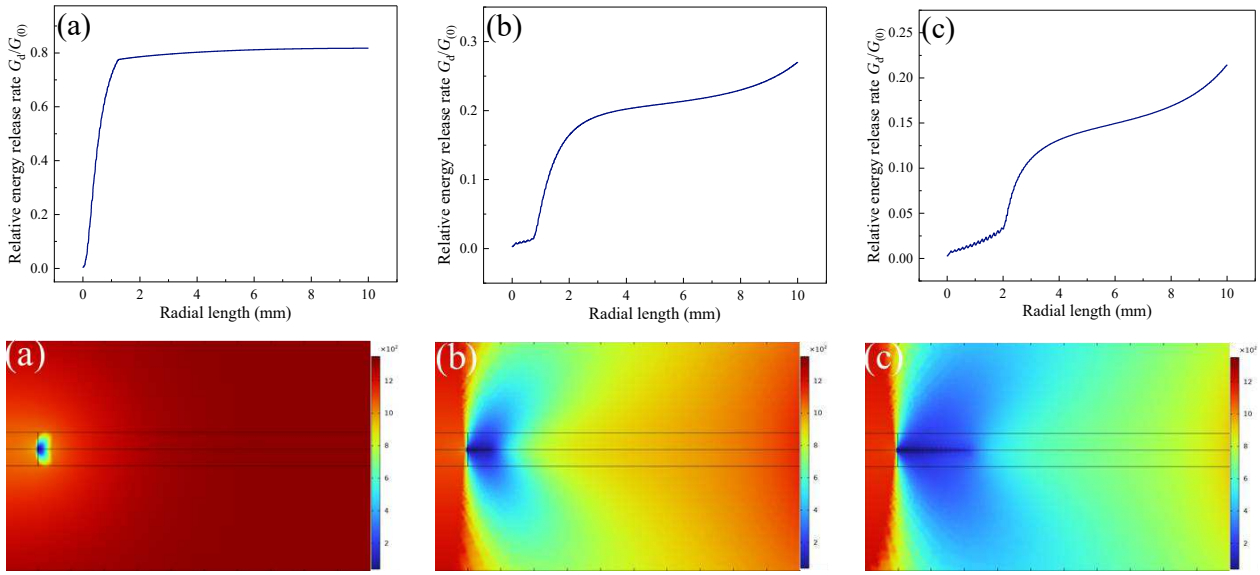


Figure 12 Variation of the energy release rate along the crack propagation direction at different stages under 5.5 MPa hydrogen pressure (a) N2, (b) N3, and (c) N4

Figure 13 shows the maximum relative critical energy release rate at each stage under different hydrogen pressures. The degradation patterns exhibit an apparent pressure-dependent transition in the model. For **low hydrogen pressures** (5.5 and 6.89 MPa), the most significant degradation occurs during **Stage II** (accelerated propagation). At 5.5 MPa, the maximum G_d/G_0 decreases from approximately 0.81 at N2 to 0.21 at N4, representing a reduction of about 74% during Stage II. At 6.89 MPa, a similar trend is observed, with the degradation concentrated in the long duration of Stage II, where fatigue cycling accumulates extensive damage over millions of cycles. Within the model assumptions, this indicates that at low hydrogen pressures, fatigue effects dominate material degradation during the prolonged accelerated propagation stage. For 21 and 34 MPa, the model shows an apparent Stage I degradation peak; these pressures lie outside the linear-elastic validity range. At 34 MPa, the maximum G_d/G_0 drops sharply from approximately 0.52 at N1 to 0.18 at N2, accounting for more than 65% of the total degradation before any macroscopic crack extension occurs. This apparent trend is therefore not used as a mechanistic conclusion because the nominal hoop stress exceeds the X52 yield strength under these pressures. No transition mechanism is claimed because the high-pressure cases lie outside the model's validity range.

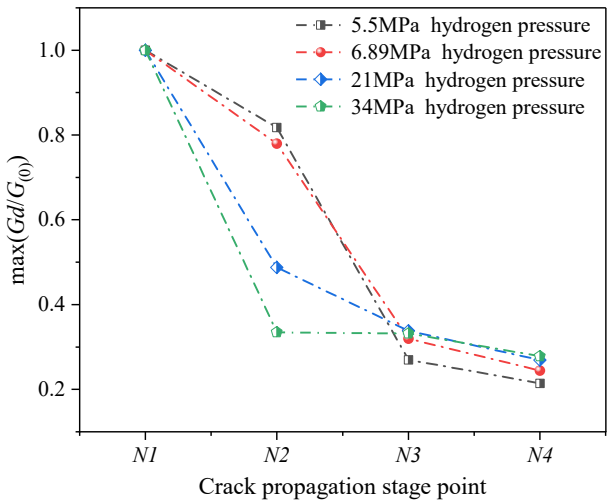


Figure 13 Evolution of the maximum relative critical energy release rate at each stage of fatigue crack propagation under different hydrogen pressures

5. Conclusions

(1) A coupled deformation-diffusion-fatigue phase-field model was implemented to simulate hydrogen-assisted fatigue crack growth in X52 pipeline steel. The model captures crack initiation and propagation without requiring predefined crack paths; coalescence is not exercised in the single-crack cases considered here.

(2) The fatigue crack propagation process is divided into three stages under the present stage definitions: Stage I (energy accumulation, ~20% of total life), Stage II (accelerated propagation, ~72%–74% of total life), and Stage III (rapid fracture, ~3%–6% of total life). The proportions are approximately consistent in the cases considered; they are definition-dependent and should not be interpreted as intrinsic material constants or design-life fractions.

(3) The relative hydrogen concentration (C/C0) evolves in a distinctive pattern in the present model: it increases towards crack initiation (N2), reaching values of 1.25–1.45 depending on hydrogen pressure, and then decreases during subsequent propagation in the simulated phase-field fields.

(4) Within the regularization scale considered in this model, the maximum hydrogen concentration is not located at the crack tip but approximately 0.1–0.2 mm ahead in the simulated phase-field fields. This migration distance increases with crack propagation and hydrogen pressure; in the present linear elastic model it is attributed to stress redistribution in the regularised crack-tip field, not to plastic blunting, and its dependence on the phase-field length has not been established.

(5) The critical energy release rate degrades by approximately 19% in the hydrogen environment at 5.5 MPa relative to the hydrogen-free baseline. Within the linear-elastic pressure range considered, maximum degradation occurs during Stage II; the 21 and 34 MPa cases are outside the model's validity range and are not used for mechanistic conclusions. The single 5.5 MPa hydrogen-free baseline provides an illustrative decomposition of hydrogen and fatigue contributions. All quantitative results require experimental validation before engineering use.

References

[1] M. Usman, K. K. A. Eric, and R. Rajakumaran, 'Hydrogen in transition: Comparative analysis of technologies, innovations, and global strategies for decarbonization', *eTransportation*, vol. 28, p. 100592, 2026, doi: https://doi.org/10.1016/j.etran.2026.100592.

[2] O. A. Zambrano, K. Ton, and A. Islam, 'Towards the understanding of hydrogen embrittlement in pipeline steels using EBSD', *Int. J. Hydrog. Energy*, vol. 174, p. 151470, 2025, doi: https://doi.org/10.1016/j.ijhydene.2025.151470.

[3] J. Zheng *et al.*, 'Research on the fatigue crack growth rate model for X80 pipeline steel in a hydrogen environment', *Int. J. Hydrog. Energy*, vol. 255, p. 156432, 2026, doi: https://doi.org/10.1016/j.ijhydene.2026.156432.

[4] A. O. Myhre *et al.*, 'Hydrogen enhanced fatigue crack growth rates in a vintage and a modern X65 pipeline steel', *Int. J. Fatigue*, vol. 201, p. 109186, Dec. 2025, doi: 10.1016/j.ijfatigue.2025.109186.

[5] M. Gyaabeng, R. Ahmed, S. Rhythm, N. Ahmed, and C. Teodoriu, 'Impacts of gas composition and temperature on the hydrogen embrittlement of pipeline steels', *Eng. Fail. Anal.*, vol. 181, p. 109964, 2025, doi: https://doi.org/10.1016/j.engfailanal.2025.109964.

[6] S. Yang, R. Darabi, A. Reis, A. de Jesus, D. Meng, and S.-P. Zhu, 'A multiphysics phase-field–diffusion framework for hydrogen-assisted fatigue crack initiation and growth in welded pipeline steels', *J. Mater. Res. Technol.*, vol. 42, pp. 5457–5474, 2026, doi: https://doi.org/10.1016/j.jmrt.2026.04.131.

[7] S. Nazar and E. Proverbio, 'Modeling of hydrogen-assisted fatigue crack growth in carbon steel pipelines', *Int. J. Hydrog. Energy*, vol. 138, pp. 548–558, 2025, doi: https://doi.org/10.1016/j.ijhydene.2025.05.205.

[8] K. Ma, R. Zhang, C. Lu, W. Peng, and J. Zheng, 'Phase field model for hydrogen-assisted fatigue crack growth considering dynamic hydrogen adsorption behavior', *Theor. Appl. Fract. Mech.*, vol. 138, p. 104960, 2025, doi: https://doi.org/10.1016/j.tafmec.2025.104960.

[9] S. Wang, A. Nagao, P. Sofronis, and I. M. Robertson, 'Assessment of the impact of hydrogen on the stress developed ahead of a fatigue crack', *Acta Mater.*, vol. 174, pp. 181–188, 2019, doi: https://doi.org/10.1016/j.actamat.2019.05.028.

[10] F. D. León-Cázares, M. Agnani, J. Ronevich, and C. S. Marchi, 'Effects of hydrogen partial pressure on crack initiation and growth rate in vintage X52 steel', *Int. J. Hydrog. Energy*, vol. 136, pp. 914–922, 2025, doi: https://doi.org/10.1016/j.ijhydene.2024.02.292.

[11] X. Xu, R. Zhang, C. Wang, C. Liu, J. Zhang, and Y. Li, 'Experimental study on the temperature dependence of gaseous hydrogen permeation and hydrogen embrittlement susceptibility of X52 pipeline steel', *Eng. Fail. Anal.*, vol. 155, p. 107746, 2024, doi: https://doi.org/10.1016/j.engfailanal.2023.107746.

[12] O. Bouledroua, D. Zelmati, Z. Hafsi, and M. B. Djukic, 'Hydrogen embrittlement effects on remaining life and fatigue crack growth rate in API 5L X52 steel pipelines under cyclic pressure loading', *Eng. Fail. Anal.*, vol. 166, p. 108917, 2024, doi: https://doi.org/10.1016/j.engfailanal.2024.108917.

[13] A. Ghasemi and H. Jafarzadeh, 'Phase-field analysis of hydrogen-assisted fracture: Effects of initial crack characteristics, hydrogen distribution, and multi-crack interactions', *Eng. Fract. Mech.*, vol. 338, p. 112002, 2026, doi: https://doi.org/10.1016/j.engfracmech.2026.112002.

[14] S. Yang *et al.*, 'Predicting high-cycle fatigue under hydrogen embrittlement with a coupled phase-field–diffusion model', *Int. J. Fatigue*, vol. 210, p. 109674, 2026, doi: https://doi.org/10.1016/j.ijfatigue.2026.109674.

[15] L. Yu *et al.*, 'Synergistic effects of temperature, stress ratio, and hydrogen on fatigue crack propagation

behavior of 7B05 aluminum alloy: a multi-physics phase-field investigation', *Theor. Appl. Fract. Mech.*, vol. 145, p. 105671, 2026, doi: https://doi.org/10.1016/j.tafmec.2026.105671.

[16] Y. Zhang, P. Xu, W. Ding, H. Jia, W. Ouyang, and F. Cheng, 'Phase-field simulation of dual-crack system hydrogen embrittlement in metallic materials', *Theor. Appl. Fract. Mech.*, vol. 131, p. 104332, 2024, doi: https://doi.org/10.1016/j.tafmec.2024.104332.

[17] Y. Chen and Y. Shen, 'Energy barrier for crack nucleation via the phase field approach to fracture and the nudged elastic band method', *Eng. Fract. Mech.*, vol. 340, p. 112107, 2026, doi: https://doi.org/10.1016/j.engfracmech.2026.112107.

[18] H. Tang, J. Shang, B. Xing, R. Gao, and Z. Hua, 'Phase field modeling of hydrogen-assisted cracking for high strength steels: Incorporating stress-state-dependent failure resistance', *Eng. Fract. Mech.*, vol. 345, p. 112442, 2026, doi: https://doi.org/10.1016/j.engfracmech.2026.112442.

[19] C. Cui, P. Bortot, M. Ortolani, and E. Martínez-Pañeda, 'Computational predictions of hydrogen-assisted fatigue crack growth', *Int. J. Hydrog. Energy*, vol. 72, pp. 315–325, 2024, doi: https://doi.org/10.1016/j.ijhydene.2024.05.264.

[20] A. Golahmar, P. K. Kristensen, C. F. Niordson, and E. Martínez-Pañeda, 'A phase field model for hydrogen-assisted fatigue', *Int. J. Fatigue*, vol. 154, p. 106521, 2022, doi: https://doi.org/10.1016/j.ijfatigue.2021.106521.

[21] H. Liu, R. Ruan, Y. Ma, and Y. Shen, 'Phase-field modelling of hydrogen-assisted fatigue cracking: Theoretical framework and numerical implementation', *Int. J. Hydrog. Energy*, vol. 158, p. 150502, 2025, doi: https://doi.org/10.1016/j.ijhydene.2025.150502.

[22] P. K. Kristensen, C. F. Niordson, and E. Martínez-Pañeda, 'Applications of phase field fracture in modelling hydrogen assisted failures', *Theor. Appl. Fract. Mech.*, vol. 110, p. 102837, 2020, doi: https://doi.org/10.1016/j.tafmec.2020.102837.

[23] E. Martínez-Pañeda, A. Golahmar, and C. F. Niordson, 'A phase field formulation for hydrogen assisted cracking', *Comput. Methods Appl. Mech. Eng.*, vol. 342, pp. 742–761, 2018, doi: https://doi.org/10.1016/j.cma.2018.07.021.

[24] A. Alvaro, I. T. Jensen, N. Kheradmand, O. M. Løvvik, and V. Olden, 'Hydrogen embrittlement in nickel, visited by first principles modeling, cohesive zone simulation and nanomechanical testing', *Int. J. Hydrog. Energy*, vol. 40, no. 47, pp. 16892–16900, 2015, doi: https://doi.org/10.1016/j.ijhydene.2015.06.069.

[25] A. Tehranchi, X. Zhang, G. Lu, and W. A. Curtin, 'Hydrogen–vacancy–dislocation interactions in α-Fe', *Model. Simul. Mater. Sci. Eng.*, vol. 25, no. 2, p. 025001, Dec. 2016, doi: 10.1088/1361-651X/aa52cb.

[26] C. Miehe, F. Welschinger, and M. Hofacker, 'Thermodynamically consistent phase-field models of fracture: Variational principles and multi-field FE implementations', *Int. J. Numer. Methods Eng.*, vol. 83, no. 10, pp. 1273–1311, 2010, doi: https://doi.org/10.1002/nme.2861.

[27] P. C. Chen, Y. E. Ma, F. Peng, and L. L. Zhou, 'Phase-field simulation of hydrogen embrittlement fracture' (in Chinese), *J. Northwestern Polytech. Univ.*, vol. 40, no. 3, pp. 504–511, 2022.

[28] J.-Y. Kim, K.-W. Seo, Y.-J. Kim, and K.-S. Kim, 'Fracture analysis of hydrogen-embrittled API X52 pipes at low temperature', *Int. J. Mech. Sci.*, vol. 276, p. 109374, 2024, doi: https://doi.org/10.1016/j.ijmecsci.2024.109374.

[29] R. Zhang, K. Ma, W. Peng, and J. Zheng, 'Effects of hydrogen pressure on hydrogen-assisted fatigue crack growth of Cr-Mo steel', *Theor. Appl. Fract. Mech.*, vol. 129, p. 104202, 2024, doi: https://doi.org/10.1016/j.tafmec.2023.104202.

Acknowledgements

The authors gratefully acknowledge the financial support from the **Xinjiang Uygur Autonomous Region Key R&D Task Special Project** (Grant Nos. 2024B01003-1 and 2024B01003-2).

Data Availability

The data that support the findings of this study are available from the corresponding author upon reasonable request.